A&A 652, A162 (2021)
https://doi.org/10.1051/0004-6361/202039751

Astronomy & Astrophysics

Milky Way spiral arms from open clusters in *Gaia* EDR3

A. Castro-Ginard[1], P. J. McMillan[2], X. Luri[1], C. Jordi[1], M. Romero-Gómez[1], T. Cantat-Gaudin[1], L. Casamiquela[3], Y. Tarricq[3], C. Soubiran[3], and F. Anders[1]

[1] Dept. Física Quàntica i Astrofísica, Institut de Ciències del Cosmos (ICCUB), Universitat de Barcelona (IEEC-UB), Martí i Franquès 1, 08028 Barcelona, Spain
e-mail: acastro@fqa.ub.edu
[2] Lund Observatory, Department of Astronomy and Theoretical Physics, Lund University, Box 43, 22100 Lund, Sweden
[3] Laboratoire d'Astrophysique de Bordeaux, Univ. Bordeaux, CNRS, B18N, allée Geoffroy Saint-Hilaire, 33615 Pessac, France

Received 23 October 2020 / Accepted 7 May 2021

ABSTRACT

Context. The physical processes driving the formation of Galactic spiral arms are still under debate. Studies using open clusters favour the description of the Milky Way spiral arms as long-lived structures following the classical density wave theory. Current studies comparing the *Gaia* DR2 field stars kinematic information of the solar neighbourhood to simulations, find a better agreement with short-lived arms with a transient behaviour.
Aims. Our aim is to provide an observational, data-driven view of the Milky Way spiral structure and its dynamics using open clusters as the main tracers, and to contrast it with simulation-based approaches. We used the most complete catalogue of Milky Way open clusters, with astrometric *Gaia* EDR3 updated parameters, estimated astrophysical information, and radial velocities, to revisit the nature of the spiral pattern of the Galaxy.
Methods. We used a Gaussian mixture model to detect overdensities of open clusters younger than 30 Myr that correspond to the Perseus, Local, Sagittarius, and Scutum spiral Arms, respectively. We used the birthplaces of the open cluster population younger than 80 Myr to trace the evolution of the different spiral arms and compute their pattern speed. We analysed the age-distribution of the open clusters across the spiral arms to explore the differences in the rotational velocity of stars and spiral arms.
Results. We are able to increase the range in Galactic azimuth where present-day spiral arms are described, better estimating its parameters by adding 264 young open clusters to the 84 high-mass star-forming regions used so far, thus increasing the number of tracers by 314%. We used the evolution of the open clusters from their birth positions to find that spiral arms nearly co-rotate with field stars at any given radius, discarding a common spiral pattern speed for the spiral arms explored.
Conclusions. The derivation of different spiral pattern speeds for the different spiral arms disfavours classical density waves as the main drivers for the formation of the Milky Way spiral structure, and it is in better agreement with simulation-based approaches that tend to favour transient spirals. The increase in the number of known open clusters, as well as in their derived properties, allows us to use them as effective spiral structure tracers and homogenise the view from open clusters and field stars on the nature of the Galactic spiral arms.

Key words. Galaxy: disk – open clusters and associations: general – astrometry – methods: data analysis

1. Introduction

The location of our Solar System within the Milky Way disc makes it challenging to obtain a detailed picture of its structure. This is particularly true for the spiral structure. The number, location, and nature of the spiral arms still remain unclear. Lin & Shu (1964) proposed a theoretical mechanism for the formation of spiral arms, widely known as the density wave theory, where the spiral arms rotate like a rigid solid at a constant angular velocity (i.e. pattern speed) in spite of the differential rotation of the stars and interstellar medium, causing the spiral arms to be long lived (see Shu 2016, for a review of the classic theory). Alternatively, Toomre (1964) proposed that spiral arms could reform short-lived structures composed by individual arms, each of them behaving as a wave at a constant pattern speed and overlapping causing transient spiral arms with no global spiral pattern speed (Quillen et al. 2011; Sellwood & Carlberg 2014). The latter short-lived arms can also be explained with material arms that co-rotate with disc stars (Wada et al. 2011; Grand et al. 2012), causing the spiral pattern to grow from local gravitational instabilities and then to disappear, with continuous instabilities regenerating the pattern again.

Since the first attempts to explain the nature of the arms almost 60 years ago, no clear conclusion has been reached. Dobbs & Baba (2014) proposed types of observational evidence to shed light on the nature of the spiral structure, based on the different rotation velocities for the spiral pattern and disc stars. These strategies include the direct derivation of the spiral pattern speed for each arm, which will help in favouring either a density wave theory, where the arms share a global constant spiral pattern speed, or a transient behaviour which shows a spiral pattern speed decreasing with galactocentric radius (Shabani et al. 2018). The distribution of ages of the stellar clusters across any spiral arm also indicates a difference in the velocities of both structures, the distribution of stars and the arm. Given the improvements on the open cluster catalogue made in light of *Gaia's* second data release (*Gaia* DR2, Gaia Collaboration 2018a), and using them as main tracers of Galactic spiral structure, both elements of observational evidence can be pursued for the first time providing a new view of the nature of the Milky Way spiral arms.

Open clusters (OCs) are excellent tracers of the spatial structure of the young stellar population in the Galactic disc. They are groups of gravitationally bound stars that were born from the

same molecular cloud and therefore have very similar positions, velocities, ages, and initial chemical compositions (Lada & Lada 2003). For an OC, the estimation of its properties such as the parallax, proper motion, radial velocity, age, or extinction is more reliable than for individual field stars because it relies on a (large) number of members, whose parameters are averaged.

Using OCs as the spiral arms' main tracers, Naoz & Shaviv (2007) found that spiral pattern speeds for the Perseus, Local, and Sagittarius spiral Arms decrease with galactocentric radius, finding evidence for multiple spiral sets. Again, using young OCs as the spiral arms' main tracers and *Gaia* DR2, Dias et al. (2019) obtained a common pattern speed for the Perseus, Local, and Sagittarius spiral Arms of $28.2 \pm 2.1\,\mathrm{km\,s^{-1}\,kpc^{-1}}$, supporting the idea of the density wave nature of the spiral structure. This results in a co-rotation radius, meaning a galactocentric radius at which the spiral pattern speed coincides with the velocity from the Galactic rotation curve, of $R_c = 8.51 \pm 0.64$ kpc. Junqueira et al. (2015) used a sample of giant stars from OCs observed by APOGEE DR10 (Anders et al. 2014) to find a pattern speed of $23.0 \pm 0.5\,\mathrm{km\,s^{-1}\,kpc^{-1}}$, with a corresponding co-rotation radius of $R_c = 8.74$ kpc, compatible with the previous result within uncertainties. However, even though R_c is a fundamental parameter in the density wave scenario, there is not a consensus on its value yet. Different studies using different tracers place it from 6.7 kpc to beyond the Perseus arm, which is located at ∼10 kpc (Drimmel & Spergel 2001; Monguió et al. 2015; Michtchenko et al. 2018).

From a complementary point of view, by comparing the kinematic substructure of field stars in the solar neighbourhood to simulated data, Hunt et al. (2018) showed that a simulated galaxy with transient spiral arms reproduces the arches and ridges seen in the velocity distribution of *Gaia* DR2 (Gaia Collaboration 2018b; Antoja et al. 2018; Ramos et al. 2018). In this transient scenario, R_c is not an important parameter since the spiral arms would co-rotate with stars at their galactocentric radii, causing short-lived arms. A number of authors looking at the field population, some using simulation-based approaches, tend to favour a transient nature for the spirals (Quillen et al. 2018; Hunt et al. 2020; Kamdar et al. 2020).

Since the publication of *Gaia* DR2, hundreds of new OCs have been detected (Castro-Ginard et al. 2018, 2019, 2020; Liu & Pang 2019; Sim et al. 2019) and have been added to the OCs that were already known and confirmed by *Gaia* DR2 (Cantat-Gaudin et al. 2018). For this compendium of OCs, information about age, distance, and line-of-sight extinction was computed (Cantat-Gaudin et al. 2020), and radial velocities were compiled from different ground-based spectroscopic surveys (Tarricq et al. 2021). Altogether, this results in a robust OC catalogue that offers the chance to trace the spiral structure of the Galactic disc (in the solar neighbourhood) and its evolution over the past few hundred Myr.

Our aim for this paper is to use this recent and homogeneous OC sample with information on astrometric mean parameters, radial velocities, and astrophysical parameters available to discriminate as far as possible among different theories for the nature of the spiral structure of the Milky Way, supporting either classical density waves or transient spiral arms.

The paper is organised as follows. In Sect. 2, we describe the OC sample that we used throughout the analysis. In Sect. 3, we study the spatial distribution of the reported OCs, particularly the youngest ones, and derive the present-day spiral arms structure. In Sect. 4, we use the astrophysical information of OCs (i.e. phase-space coordinates and ages) to test the density wave nature of the spiral arms, by computing the spiral pattern speed for the Perseus, Local, Sagittarius, and Scutum spiral Arm segments. In Sect. 5, we explore the imprints left in the age distribution of the open clusters across the spiral arms by the differences in the rotational velocity of the stars and the arms. The discussion on the results obtained can be found in Sect. 6, and our conclusions are given in Sect. 7.

2. The open cluster sample

The data used throughout the paper are those from the OCs identified in *Gaia* DR2 (Gaia Collaboration 2018a), with their mean astrometric values updated with *Gaia* EDR3 measurements (Gaia Collaboration 2021). The use of OCs allows us to have better constrained parameters than using field stars. The parameters needed for our methodology are the mean astrometric parameters, meaning $(l, b, \mu_{\alpha^*}, \mu_\delta)$; the astrophysical parameters derived from *Gaia* astrometry and photometry, which are OC age, distance and line-of-sight extinction (Cantat-Gaudin et al. 2020); and radial velocity measurements for each OC (Tarricq et al. 2021).

2.1. Gaia EDR3 astrometry

The sample of OCs used in this work includes those known prior to (and that were confirmed by) *Gaia* DR2 (Cantat-Gaudin et al. 2018). Additionally, we have included the large number of clusters which have been found in *Gaia* DR2 data (e.g. Castro-Ginard et al. 2018, 2019, 2020; Sim et al. 2019; Liu & Pang 2019). We updated the OC mean astrometric parameters with the *Gaia* EDR3 astrometric information, in which measurements are more precise given the longer time baseline for the observations. In total, there are 2017 OCs in these catalogues. For those clusters, we used the sky coordinates and proper motions for the centre of the OC $(l, b, \mu_{\alpha^*}, \mu_\delta)$, which were computed from its member stars. The uncertainties in the position (l, b) can be neglected. The uncertainties in the mean proper motions are below $0.2\,\mathrm{mas\,yr^{-1}}$, generally around $0.1\,\mathrm{mas\,yr^{-1}}$.

2.2. Age, distance, and line-of-sight extinction

Cantat-Gaudin et al. (2020) published a catalogue of ages, distances, and line-of-sight extinctions for the OCs known to date. They used an artificial neural network to infer these parameters for each OC from its colour-magnitude diagram (CMD) in the *Gaia* passbands $(G, G_{\mathrm{BP}}, G_{\mathrm{RP}})$ and parallax information (ϖ). The authors were able to compute these astrophysical parameters for 1878 of the 2017 OCs reported. For the 139 others, the OC had too few members or its CMD was too red, and no reliable estimation could be obtained using *Gaia* data alone.

The uncertainties in those quantities depend on the number of cluster members (see Sect. 3.4 of Cantat-Gaudin et al. 2020, for details). We took the one sigma uncertainty for the age as $\sigma_{\log t} \in [0.15, 0.25]$ dex, which are the values for the young OCs' uncertainties recommended by Cantat-Gaudin et al. (2020). The uncertainty on the distance modulus is from 0.1 to 0.2 mag, corresponding to a 5%−10% distance uncertainty. Cantat-Gaudin et al. (2020) reported that they found no systematic effects on the determination of the parameters with respect to the literature.

2.3. Radial velocities

Radial velocities used in this work are those compiled by Tarricq et al. (2021). The authors crossmatched the OC members

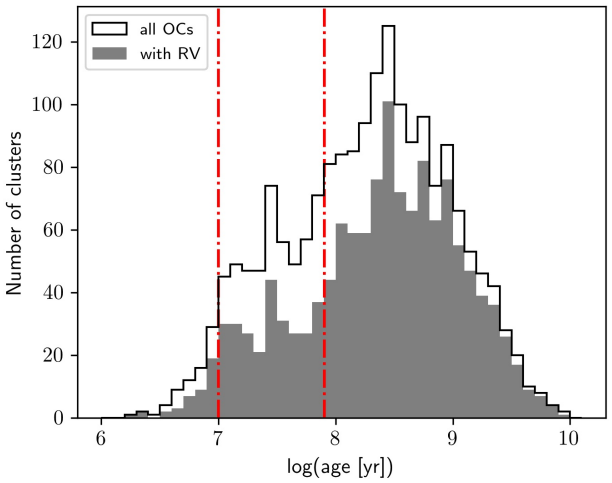

Fig. 1. Histogram of OC ages. Solid line shows OCs with age estimation available, whilst solid bars show the subset of OCs with radial velocity measurements. Red dash-dotted vertical lines correspond to 10 and 80 Myr.

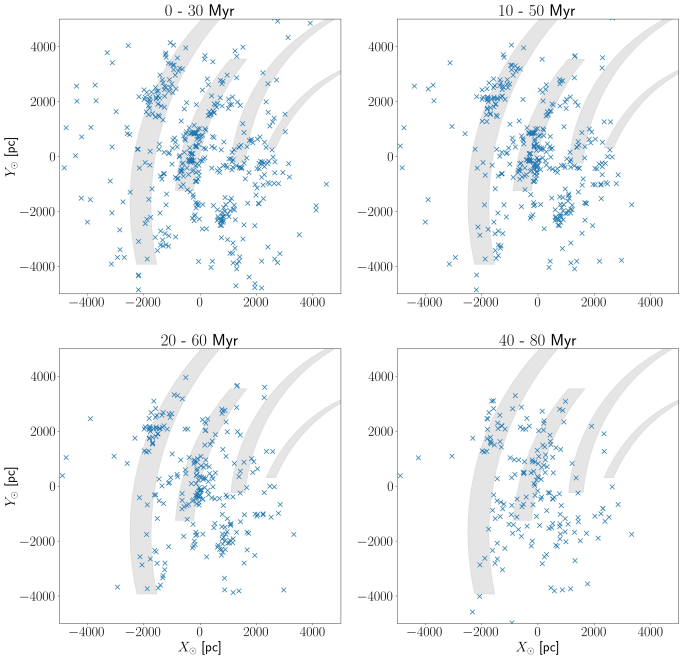

Fig. 2. Distribution of OCs in heliocentric X–Y in different age bins. The Galactic centre is towards positive X values, and the direction of the Galactic rotation is towards positive Y values. Blue crosses are OC with age estimations; regardless of whether they have available radial velocity measurements or not, *from left to right* and *from top to bottom* they correspond to: ages below 30 Myr, from 10 to 50 Myr, from 20 to 60 Myr, and from 40 to 80 Myr. The spiral arms defined by Reid et al. (2014) are overplotted.

with several radial velocity catalogues. In addition to *Gaia*-RVS (Katz et al. 2019), they used data from ground-based large spectroscopic surveys: the latest public version of the *Gaia*-ESO survey (Randich et al. 2013), APOGEE DR16 (Ahumada et al. 2020), RAVE DR6 (Steinmetz et al. 2020), and GALAH DR2 (Buder et al. 2018; Zwitter et al. 2018). They also included data from other radial velocity catalogues: Nordström et al. (2004), Mermilliod et al. (2008, 2009), Worley et al. (2012), the OCCASO survey (Casamiquela et al. 2016), and Soubiran et al. (2018).

This catalogue consists of radial velocity estimates for 1382 clusters, with 1321 of them having astrophysical parameters estimated by Cantat-Gaudin et al. (2020). The median radial velocity uncertainty of the full catalogue is 1.13 km s^{-1}. We refer the reader to the original paper for the details concerning the computation of the cluster radial velocities.

2.4. Final OC sample

Figure 1 shows the distribution of ages of the two sub-samples of OCs. The one with age, distance, and line-of-sight extinction determination is represented as a solid black line; whilst the grey bars represent the clusters with radial velocity measurements. The red dash-dotted lines correspond to ages equal to 10 and 80 Myr, and they show the subset of OCs that we used to compute the spiral pattern speed in Sect. 4.

3. Present-day OC spatial distribution

The spiral pattern is clearly seen in a heliocentric X–Y projection of the OCs with ages below 150 Myr (see Fig. 8 and Fig. 1 of Cantat-Gaudin et al. 2020; Kounkel et al. 2020, respectively), while for older bins this pattern disappears. Further dividing this 0–150 Myr range in four bins, we are able to spot the OCs' overdensities corresponding to the spiral arms in a range of ages. This traces the evolution of the spiral pattern during the time interval where the overdensities are seen (see Sect. 4.2). Figure 2 shows how spiral arm segments in the solar neighbourhood are clearly seen in OC overdensities for the youngest age interval explored (0–30 Myr) and how these overdensities show an increasing dispersion with time, and hence a slow dilution. The black shaded regions represent the spiral arms as modelled by Reid et al. (2014).

Re-determination of current spiral arms

We re-determined the parameters of the present-day spiral arms using the hypothesis that OCs are born in spiral arms (Roberts 1969) and that the youngest OCs (≤30 Myr) have not moved far from their birth places (Dias & Lépine 2005). Thus, considering the usual log-periodic spiral arms, each arm should be detected as an overdensity following the relation used by Reid et al. (2014):

$$\ln \frac{R_G}{R_{G,\mathrm{ref}}} = -(\theta_G - \theta_{G,\mathrm{ref}}) \tan \psi, \tag{1}$$

where R_G and θ_G are galactocentric radius and azimuth along the arm, respectively. $R_{G,\mathrm{ref}}$, $\theta_{G,\mathrm{ref}}$ (taken to be near the median value of θ_G), and ψ are a reference galactocentric radius and azimuth, and the pitch angle for a given arm. The galactocentric azimuth is taken to be $\theta_G = 0$ on the Sun-Galactic centre line, and growing towards the Galactic rotation direction.

We detected the overdensities using a Gaussian mixture model (GMM) in the $(\ln R_G, \theta_G)$ space. A GMM is able to describe all the points in the parameter space as a weighted sum of Gaussians. This representation of our sample allows us to describe each arm, expected to follow Eq. (1) with some dispersion, as a Gaussian in that direction (straight line in the $(\ln R_G, \theta_G)$ space). The number of Gaussians to fit is automatically selected using the Bayesian information criterion (BIC).

Once the Gaussian field was obtained, we selected the Gaussian components with the four highest weights, corresponding to

Table 1. Fitted parameters, including statistical errors, for present-day spiral arms.

Arm	$N_{\rm tracers}$ OC+HMSFR	$\theta_{G,\rm ref}$ [deg]	$\theta_{G,\rm range}$ [deg]	$R_{G,\rm ref}$ [kpc]	ψ [deg]
Perseus	56 + 24	−13.0	(−20.9, 88.2)	10.88 ± 0.04	9.8 ± 0.9
Local	121 + 25	−2.3	(−26.9, 26.6)	8.69 ± 0.01	8.9 ± 1.3
Sagittarius	61 + 18	3.5	(−39.3, 67.7)	7.10 ± 0.01	10.6 ± 0.8
Scutum	26 + 17	−4.8	(−32.7, 100.9)	6.02 ± 0.02	14.9 ± 1.6

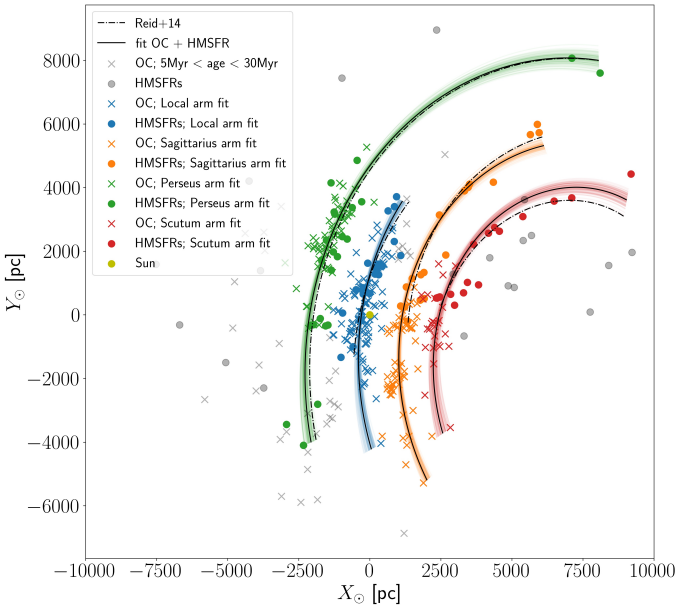

Fig. 3. Heliocentric X–Y distribution of OCs (crosses) younger than 30 Myr and HMSFRs (dots) from Reid et al. (2014), used to fit the spiral arms. Different colours correspond to different arms. The assignments to each arm are computed using a GMM. Solid black lines are the fitted spiral arms with the parameters in Table 1, while shaded regions account for 1σ uncertainties. Dash-dotted lines correspond to the spiral arms defined by HMSFRs only. The Galactic centre is towards positive X and the Galactic rotation direction is towards positive Y.

the four arm segments. We find 56, 121, 61, and 26 OCs younger than 30 Myr assigned to the Perseus, Local, Sagittarius, and Scutum Arms, respectively. To increase the number of spiral arm tracers and be able to trace the arm in a wider range of Galactic azimuth, we included the data from Reid et al. (2014) used to fit the spiral arms. These data correspond to 103 high-mass star-forming regions (HMSFRs) with parallax and proper motion measurements obtained using very-long-baseline interferometry (VLBI) techniques, 84 of which are assigned to one of the four explored spiral arms. In order to obtain the parameters for each arm, we fitted Eq. (1) to the OCs and HMSFRs assigned to each arm by the minimum least-squares method (348 tracers in total, 264 OCs and 84 HMSFRs). The parameters obtained for each arm are listed in Table 1.

Figure 3 shows the representation of the spiral arms defined by the OCs and HMSFRs. The black solid lines correspond to the best-fit value for each arm, and the shaded regions correspond to the 1σ uncertainty taken into account from the correlations among the estimated parameters. Our all-sky OC sample provides a good complement to the ground-based observations used by Reid et al. (2014), who did not cover the fourth quadrant. By increasing the number of total tracers by factor of 4, we can better constrain the estimation of the mean galactocentric radius (R_G) and pitch angle (ψ), finding lower uncertainties in these values as well as increasing the θ_G range where the arms are defined. The spiral arms defined by Reid et al. (2014) using HMSFRs are shown via dash-dotted lines to compare them with our definition, for which we use both young OCs and HMSFRs.

4. Spiral pattern speed

The spiral pattern speed is indicative of the nature of the spiral arms. As described in Gerhard (2011), the most direct way to estimate the pattern speed of the spiral arms is through the OC population, due to the robustness with which their parameters can be estimated, by averaging over their members. With the assumption that the OCs are born in spiral arms (Roberts 1969) and integrating the present OCs' positions back to their birthplaces, it is possible to compute the rotation rate at which a spiral arm has moved to reach its present-day position.

To allow for the orbit integration, we used the OC sample with radial velocity measurements available (see Fig. 1 for reference). We computed the birthplace of the OCs by integrating backwards in time following each OC orbit. The orbits were integrated following a gravitational potential composed by a spherical nucleus and bulge, a Navarro-Frenk-White dark matter halo, and a Miyamoto-Nagai disc, where its parameters have been adapted to follow the observed rotation curve of the Milky Way (Bovy 2015). The numerical processing is done using the Python package `GALPY` (Bovy 2015), which uses a Leapfrog integration scheme to trace back the orbits in time steps of 0.1 Myr. The determination of the uncertainties on the birth position is done via Monte Carlo sampling from the uncertainties on the age of each OC, which is the biggest source of error in our case (see description of the OC sample in Sect. 2). The assumed values to normalise the rotation curve for the integration are $R_\odot$ = 8.178 kpc (Gravity Collaboration 2019) and $Z_\odot$ = 20.8 pc (Bennett & Bovy 2019) for the solar position and the solar motion of $U_\odot$ = 11.1, $\Theta_0 + V_\odot$ = 248.5, $W_\odot$ = 7.25 km s^{-1} (Schönrich et al. 2010; Reid & Brunthaler 2020).

It is important to note that the birth position of each OC reveals the location of a spiral arm at a time equal to the birth time of the OC. Similarly to the method described in Dias & Lépine (2005), the arm at this previous epoch is rotated forward with a rotational velocity equal to the pattern speed of that arm, Ω_p, during a time equal to the age of the OC. We considered each arm to have a unique pattern speed, which was constant during the whole time interval considered, and free to be different from other arms' pattern speeds.

The procedure to compute the pattern speed Ω_p that best describes the data for each arm is as follows:

1. Detect overdensities that correspond to the Perseus, Local, Sagittarius, and Scutum spiral Arms (see Sect. 3). Study each arm separately.
2. Integrate each OC orbit backwards to find its birthplace. These OC birthplaces represent the location of the spiral arm at the time the OC was born.
3. Rotate past the location of the arm with a circular motion at a given pattern speed (Ω_p) during the age of the cluster (t) to find its expected present-day location, meaning $\theta_{G,\rm now} = \theta_{G,\rm birth} + \Omega_p * t$.
4. Iterate over Ω_p to find the optimal value by minimising the distance of the recovered present-day locations of the spiral arms to their analytical present-day description. The

minimisation is done in the present day to avoid having multiple spiral arm representations for multiple ages (one for each OC).
5. Repeat the procedure for 1000 Monte Carlo realisations to account for the uncertainties in the birthplace of the OC.
6. For each arm, report the best value for Ω_p as the mean value of all the pattern speeds obtained, with the standard deviation as its dispersion.

4.1. Test simulation

To test our ability to recover the pattern speed, we set up a basic simulation following the evolution of both a density wave spiral pattern and the objects born in it. We generated a log-periodic spiral arm with the parameters taken from Reid et al. (2014, Table 2, Local Arm), which we consider to be the present-day position. In this case, the actual spiral arms are described using the parameters found by Reid et al. (2014), and not our own estimation (Table 1); this is because we want to keep the position of the spiral arm and its velocity defined by independent tracers (by HMSFR and OCs, respectively). We rotated the arm backwards, keeping its shape parameters unchanged, at a constant pattern speed that we set. At times $T = 10, 20, 30, 40, 50$, and 60 Myr, a set of simulated clusters (equivalent to OCs) is generated and used as tracers of the spiral pattern speed.

Firstly, we tested the effect of the definition of the present-day spiral arm on the determination of its pattern speed, in the ideal case of the OCs moving with circular orbits (Test 1). We let the simulated clusters with different ages evolve to their present-day position with circular orbits using the Milky Way rotation curve from Bovy (2015). In this case, the spiral pattern speed is fixed at 50 km s^{-1} kpc^{-1}, while the mean circular velocity of the simulated clusters is 26.37 ± 1.91 km s^{-1} kpc^{-1}. Figure 4 shows the capabilities of the method to compute the spiral pattern speed when the present-day spiral arm is defined by i) independent means (HMSFR), or ii) the youngest simulated clusters. In the first case (blue dots), the imposed value for the spiral pattern speed (black dash-dotted line) is always recovered. In the second case (green dots), we recover the value for the circular velocity (red dotted line) when the exact same tracers are used to define the present-day spiral arm and its pattern speed. However, we can asymptotically approach the true value when older tracers are considered for the spiral pattern speed computation. From Test 1, we learn that the tracers to define the present-day spiral arms should be independent of the tracers used to compute their pattern speed. This is achieved by defining the present-day spiral arms using the HMSFRs reported in Reid et al. (2014), which are younger than 10 Myr, and using OCs older than 10 Myr to compute the spiral pattern speed.

Secondly, we tested whether the methodology is able to distinguish two different spiral pattern speeds in a more realistic situation (Test 2). The simulated clusters are now evolved using circular velocities and non-zero peculiar velocities, which are drawn from a Gaussian distribution $\mathcal{N}(0, 5)$ km s^{-1}. We also added errors to the age of the simulated clusters, consistently with those in our catalogues (see Sect. 2.2). We used the method for spiral pattern speeds of 20 and 50 km s^{-1} kpc^{-1} and assumed that the present-day spiral arm is known from independent tracers, which are HMSFRs. In Fig. 4, we show the obtained values for the two different experiments. We can recover the imposed pattern speed with a systematic error that ranges from 0.8 to 6 km s^{-1} kpc^{-1} for these different cases of Ω_p. From Test 2, we see that even though the accuracy is not enough to recover the exact individual pattern speeds, the methodology is accurate enough to differentiate between two scenarios: the 20 and the 50 km s^{-1} kpc^{-1} cases.

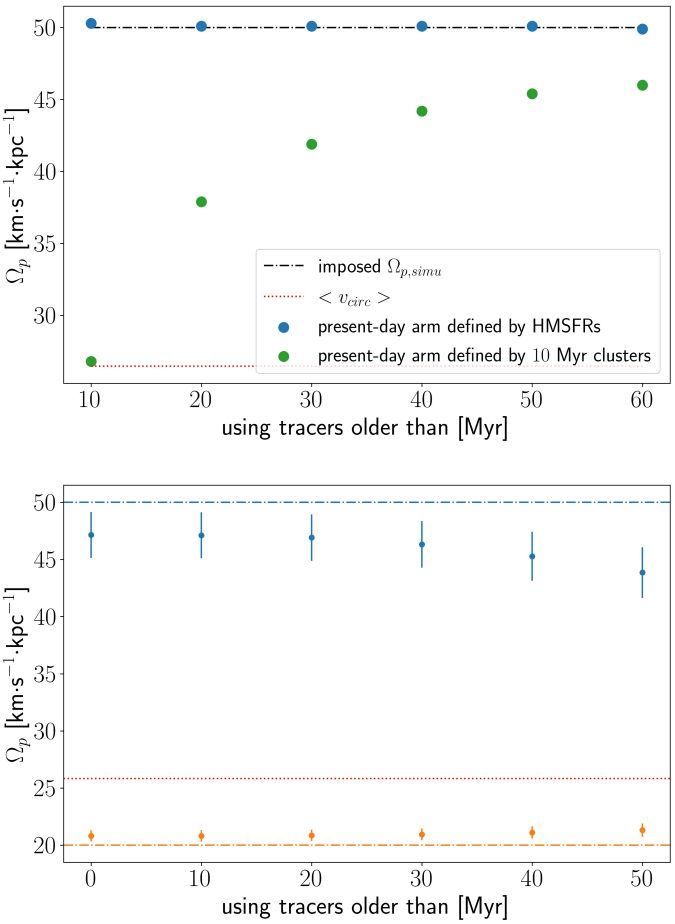

Fig. 4. Recovered Ω_p for two tests. The y-axis represents the value of the pattern speed, and the x-axis represents the minimum age of the stellar objects considered for the computation; hence, for $x = 10$ we consider objects with age ≥10 Myr. The dash-dotted lines represent the imposed value and dots represent the recovered value. The dotted red line shows the mean circular velocity of the stellar objects. *Panel a*: Test 1. Imposed $\Omega_p = 50$ km s^{-1} kpc^{-1}. Blue dots show the recovered Ω_p value when considering the present-day spiral arm defined by the HMSFRs, while green dots represent the recovered value when the present-day arm is defined with 10 Myr clusters. *Panel b*: Test 2. Pattern speed obtained for the cases of $\Omega_p = 20$ and 50 km s^{-1} kpc^{-1}: orange and blue, respectively. Dots show the recovered value, including error bars.

4.2. Estimation of Ω_p

As seen in the test simulations, the success of the methodology relies on the ability to define the present-day spiral structure by tracers other than OCs, which are used to trace the spiral pattern speed. As already mentioned, we consider that this is achieved by describing the present-day spiral structure with the HMSFRs reported in Reid et al. (2014), and therefore we used this definition of the present-day spiral arms to compute Ω_p. The authors provide the parameters from a fitting using 84 HMSFRs, younger than 10 Myr, with parallax and proper motion measurements from VLBI, as is said in Sect. 3. This information is available for the Perseus, Local, Sagittarius, and Scutum Arms. Reid et al. (2019) updated the spiral arms parameters by allowing kinks in the arm that change the pitch angle at a given θ_G.

Table 2. Pattern speed (in km s^{-1} kpc^{-1}) obtained for different age bins for each spiral arm analysed.

Arm	Ω_p (10−50 Myr)	Ω_p (20−60 Myr)	Ω_p (40−80 Myr)	Ω_p (10−80 Myr)
Perseus	17.82 ± 2.98	18.52 ± 2.60	21.66 ± 2.57	21.25 ± 2.16
Local	33.76 ± 0.94	34.31 ± 1.00	30.92 ± 0.85	31.85 ± 0.77
Sagittarius	26.10 ± 4.05	29.68 ± 3.49	26.47 ± 2.18	26.52 ± 2.03
Scutum	49.81 ± 1.90	47.67 ± 2.39	46.43 ± 2.24	46.85 ± 1.73

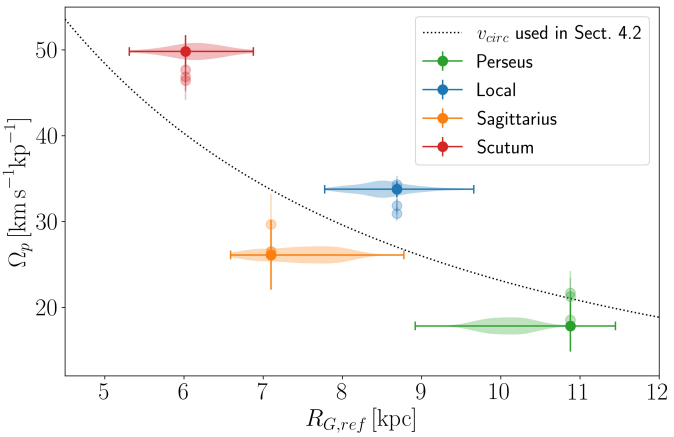

Fig. 5. Computed spiral pattern speed for the Scutum, Sagittarius, Local, and Perseus Arms (from left to right). Solid dots show the first column in Table 2, corresponding to a 10−50 Myr interval. The transparent dots are for the rest of the columns. The shaded violin plots in the x-axis show the distribution of R_G for the OCs in the 10−50 Myr interval. The dotted line shows the circular velocity from the Milky Way rotation curve. The estimated Ω_p values show a decreasing trend with galactocentric radius.

This effect is small for most of the arms we analysed, meaning there is no pitch angle variation in the Local Arm and the variations in the Perseus and Scutum Arms are within the uncertainties. Since these updates do not lead to significant changes in our calculations, we used the Reid et al. (2014) model for simplicity.

Once the present-day spiral arms are defined, we have to find the present position of the OCs born in each of these arms. In the density wave theory, the OCs may have evolved differently from their mother spiral arms, *i.e* OCs move at a velocity approximately given by the Milky Way rotation curve, while the spiral pattern moves at Ω_p. Even though the evolution follows different paths, an overdensity of very young OCs in (R_G, θ_G) will come from the same arm (see Fig. 2). As described in Sect. 3, the OCs belonging to each of the arms are selected using a GMM in the $(\ln R_G, \theta_G)$ space.

We applied the described methodology to the OCs younger than 80 Myr for different age ranges to account for the effects seen in Test 1 of Sect. 4.1. Table 2 shows the computed spiral pattern speed for the four spiral arms explored, and they show a similar trend as in the test simulation scenario. Following the same argument, we can say that the methodology is good enough to distinguish among different true spiral pattern speeds.

The recovered values for Ω_p, shown in Fig. 5, are decreasing as the galactocentric reference radius ($R_{G,\mathrm{ref}}$) of the spiral arm increases. The Ω_p for the explored arms decreases closely following the Galactic rotation curve which is represented by the dotted line, except for the case of the Local Arm, which breaks this trend. This can be related to the fact that the Local Arm could be considered not a long arm but a small armlet or a growing arm instead; however, this deserves further study (Xu et al. 2016; Liu et al. 2017; Eilers et al. 2020). Our results are in agreement with the findings of Quillen et al. (2018), who estimated the spiral pattern speeds for different spiral features to explain the arcs and ridges seen in the velocity distribution of the solar neighbourhood in *Gaia* DR2. The authors studied how the orbits of known moving groups could be perturbed by the presence of a spiral arm, and found that a spiral arm segment in the outer disc located at ∼2 kpc from the Sun with a pattern speed of 20 ± 3 km s^{-1} kpc^{-1} could be responsible for the outer boundary of the Sirius/UMa moving group. This finding is in agreement with the spiral speed of the Perseus arm segment we computed using OCs as the main tracers, with a Ω_p = 17.82 ± 2.98 km s^{-1} kpc^{-1} at a galactocentric radius of 10.88 kpc. Our results for the rest of the spiral arm segments explored are in a similar agreement (see Table 1 from Quillen et al. 2018), also for the case of the Local Arm where the authors found a pattern speed higher than the angular velocity from the rotation curve. The spiral pattern speed decreases with galactocentric radius, and spiral arms nearly co-rotate with Galactic rotation, as expected if the spiral arms are short-lived transient structures (Grand et al. 2012; Kawata et al. 2014).

5. Cluster ages across the spiral arms

The analysis of the distribution of the OCs as a function of age across a given arm can provide clues to the nature of the spiral arms (Dobbs & Baba 2014), and therefore it offers an independent approach to support the findings of the previous section. As studied by Dobbs & Pringle (2010), the differences in the rotational velocity of the stellar distribution and the spiral arms lead to different distributions of the OCs across the present-day spiral arms. Such distributions depend on the spiral arm formation mechanisms. The authors considered a set of four simulations where the spiral structure has been excited by different possible mechanisms: i) a global density wave, ii) a central rotating bar, iii) a flocculent spiral, or iv) tidally induced arms. They also discussed the potential age distribution of the clusters across a given spiral arm in each of the explored cases. A density wave and/or bar-induced spiral arms yield a trend in age across the arms. Flocculent or tidally induced mechanisms yield several individual peaks across the arm, with no age gradient. This age gradient, in the density wave or bar-induced-spirals scenario, is due to the difference in velocity with which the different structures (spiral pattern and clusters) are moving, while the spiral pattern moves with a fixed, constant-pattern speed, and the clusters move following the Galactic rotation curve. That results in older (younger) clusters leading the spiral arm if the clusters are inside (outside) the co-rotation radius. In the opposite case, for the flocculent and tidally induced arms where the spiral pattern and the stars move at roughly the same speed, the section of the arm contains clusters of different ages with no clear gradient across the arm.

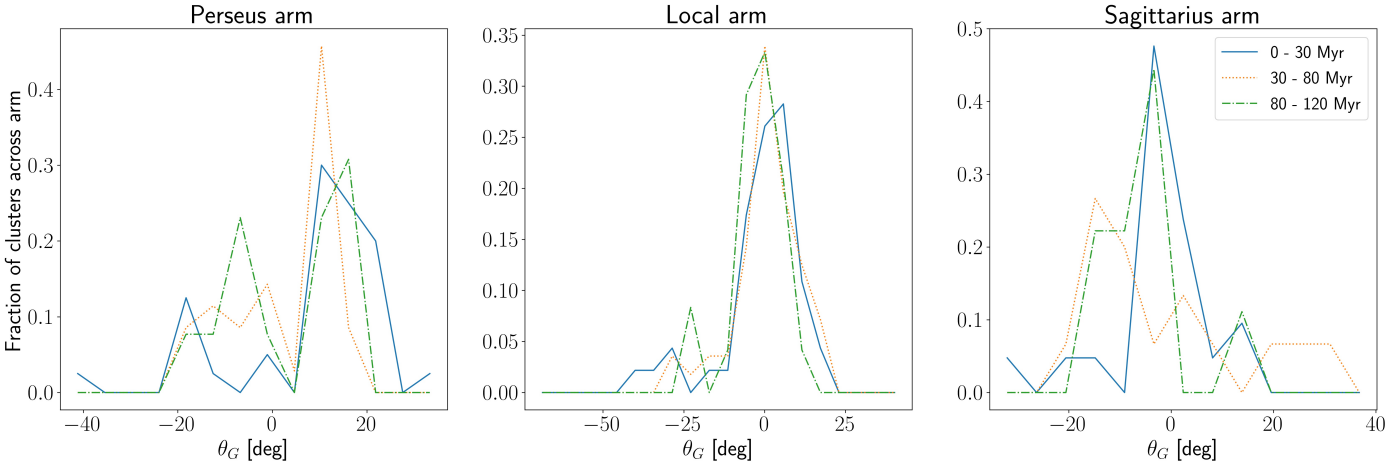

Fig. 6. Fraction of OCs for different age bins across the Perseus (*left*), Local (*middle*), and Sagittarius (*right*) Arms. The x-axis represents the Galactic azimuth (θ_G) explored for a circular section centred at the Galactic centre, at a distance of 10 (*left*), 8.3 (*middle*), and 7 (*right*) kpc. The y-axis gives the number of OCs in each θ_G bin over the total number of OCs in the whole circular section. Solid blue lines, dotted orange lines, and dash-dotted green lines correspond to clusters in 0−30 Myr, 30−80 Myr, and 80−120 Myr age bins. The numbers of OCs in each panel for the 0−30 Myr, 30−80 Myr, and 80−120 Myr age bins are as follows: 40, 35, and 13 for the Perseus Arm; 46, 56, and 24 for the Local Arm; and 21, 15, and 9 for the Sagittarius Arm, respectively.

In Fig. 6, we show a plot reproducing Fig. 4 of Dobbs & Pringle (2010) but using our OCs sample. The different panels show histograms of the number of OCs, for different cluster ages, across a circular section (500 pc wide) located at distances of 10 kpc, 8.3 kpc, and 7 kpc from the Galactic centre, meaning approximately along the Perseus, Local, and Sagittarius Arms, respectively. None of the arms show the aforementioned age gradient, which should be clearer as we move away from a hypothetical co-rotation radius. This indicates that the velocity of the clusters, meaning the stellar distribution velocity, is very similar to the rotation velocity of the spiral arms, and therefore co-rotates with them. We explored different sizes of the age bins, reaching the same conclusion in all cases. The absence of the age gradient favours the flocculent spirals or the external tidal interaction, where spiral arms tend to be transient, as the mechanisms for the excitation of the spiral structure.

The completeness of the OC population may play a role in the interpretation of Fig. 6. Castro-Ginard et al. (2020) tested how many known (prior to *Gaia*) OCs could be recovered using their detection algorithm. This recovery fraction was then used by Anders et al. (2021) to estimate the completeness of the OC population as a function of age, finding that the recovered fraction of OCs is $\lesssim$60% for the very young OCs (in the range of 1−10 Myr) and reaches $\gtrsim$90% for older OCs. Therefore, even if the fraction of youngest population in Fig. 6 may be underestimated, the older populations (defining the age gradient) are nearly complete, reaching the same conclusions of no age gradient at all.

6. Discussion

The nature of the spiral arms has been studied in other galaxies, taking advantage of our external point of view. Shabani et al. (2018) studied the distribution of stellar clusters across the spiral arms in NGC 1566, M 51, and NGC 628. They find an age gradient across the arm only in NGC 1566 (a grand design spiral galaxy with a strong bar), which is compatible with the density wave scenario (Dobbs & Pringle 2010). For the case of M 51, the spiral structure is excited by the tidal interactions with its companion, and for NGC 628 the spiral arms are consistent with a pattern speed decreasing with radius, both leading to a transient spiral nature. Also in external galaxies, the measurements of spiral pattern speeds that vary as a function of radius (Meidt et al. 2008; Speights & Westpfahl 2012) or the evolution of the spiral arms' pitch angle (Pringle & Dobbs 2019), support a transient nature for their spiral structure. This transient behaviour of the spiral structure, with the arms co-rotating with disc stars, is also expected from N-body simulations for unbarred galaxies or galaxies with a weak bar (Roca-Fàbrega et al. 2013); while galaxies with a strong bar quickly develop a spiral pattern of which the speed is constant with the radius, behaving as a global density wave as for the case of NGC 1566.

For the case of the Milky Way, the lack of a homogeneous OC catalogue (before *Gaia*) prevented us from reaching a firm conclusion (Monguió et al. 2017). Thanks to the *Gaia* mission, the study of OCs has reached maturity in terms of purity and homogeneity of the catalogue, and robustness of its estimated parameters, which allows us to apply different approaches to revisit the spiral nature of the Milky Way.

We explored the nature of the spiral structure of the Milky Way by comparing the angular velocities in which the stellar distribution and the spiral pattern move. The spiral arms should move with a global constant pattern speed in the density wave scenario, regardless of the galactocentric reference radius of the arm. This is not what we deduce from our sample of young OCs as main tracers. We see that different spiral arm segments move with a different angular velocity, which tends to decrease with their galactocentric reference radius. This behaviour is related to a short-lived transient spiral structure.

The procedure applied in this work to compute the spiral pattern speed uses the hypothesis of spiral arms with a constant shape during the time interval explored. Our tests using simulations show that the methodology is accurate enough to discard a unique pattern speed for all the spiral arms studied. The computed Ω_p values for the arms are discrepant in more than 5σ for all the arms, except for the case of the Sagittarius with Local Arms and Sagittarius with Perseus Arms, where the discrepancy is of 1.8σ and 1.6σ, respectively. For these cases, the uncertainty weighted mean of the Ω_p values is $32.03 \pm 0.87\,\mathrm{km\,s^{-1}\,kpc^{-1}}$. Therefore, we consider each arm to have its own spiral pattern

speed, which is also supported by the age gradient of the OC seen across the spiral arms studied in Sect. 5. This is in contrast with the work done by Dias et al. (2019), who used the same methodology to report a spiral pattern speed of $\Omega_p = 28.2 \pm 2.1\,\mathrm{km\,s^{-1}\,kpc^{-1}}$, common for all the explored spiral arms. Here, the inclusion of hundreds of newly discovered OCs (Castro-Ginard et al. 2020), with an updated estimation of ages, distances, and line-of-sight extinctions for the whole OC sample (Cantat-Gaudin et al. 2020), along with radial velocities for a large fraction of them (Tarricq et al. 2021) and robust statistical methodology, allows us to distinguish among different true pattern speeds for different spiral arms (Fig. 5, Table 2).

The effects that may change the shape of the spiral arms (e.g. the shear of the Galactic disc or the evolution of the pitch angle) are not included in the assumptions of this work, nor in works using similar procedures (Dias & Lépine 2005; Junqueira et al. 2015; Dias et al. 2019). However, if we consider that these effects are small over the course of ~50 Myr, the values obtained for the spiral pattern speeds suggest that spiral arms are structures that co-rotate with stars at any radii, revealing a transient nature of these arms (Grand et al. 2012). Therefore, our results with OCs agree with other works dealing with the kinematic substructure in the solar neighbourhood. These works, some including simulations, tend to explain the kinematics of moving groups or features in the action-angle space, with a transient behaviour of the Galactic spiral arms (Quillen et al. 2018, 2020; Hunt et al. 2018; Sellwood et al. 2019).

In addition, we explored the imprint in the age-distribution of the OCs across the spiral arms, and we do not see the predicted age gradient of density wave or bar-driven spiral arms (Dobbs & Pringle 2010), even when the effects due to the incompleteness of our OC sample are taken into account. The combination of both results allow us to favour a flocculent Milky Way with transient spiral arms, disfavouring the density wave scenario with a grand design morphology. This idea of a flocculent Milky Way was already studied by Quillen (2002), who found multiple spiral features, each with a different pattern speed decreasing with galactocentric radius. From the morphology of the spiral arms, a flocculent Milky Way was favoured by Xu et al. (2016) due to a long Local Arm located between the Perseus and Sagittarius Arms, which could not be explained by a density wave theory with a pure grand design morphology. *N*-body simulations are also in agreement with density waves not explaining the spiral structure in our Galaxy (Honig & Reid 2015).

7. Conclusions

We analysed the OC population with *Gaia* EDR3 astrometric parameters, radial velocities compiled from different surveys, and astrophysical parameters computed from *Gaia* DR2 astrometry and photometry, in order to derive the structure of the spiral arms in the solar neighbourhood and to discriminate among several hypotheses about their nature.

We show that each of the four investigated arms exhibits a different pattern speed. Using a combination of statistical and data-mining techniques, we find that each spiral arm has a spiral pattern speed that tends to decrease with galactocentric radius, following the Galactic rotation curve and favouring transient behaviour for these arms.

We analysed the age-distribution of the OC population across the spiral arms to see the imprint of the different angular velocities of the stellar distribution and the spiral arm segments, if any. We see no indication of the age gradient predicted by Dobbs & Pringle (2010) to be a sign of a density wave-like footprint, thus favouring a flocculent Milky Way.

These two independent experiments, based on the most complete OC sample to date, allow us to disfavour the density wave theory of spiral structure and point towards a transient nature of the spiral arms. This behaviour is seen here for the first time using OC data. This is thanks to the increase of data available in the OC sample, with radial velocities available and better estimations of ages and distances. This points in the same direction as the conclusions obtained by other authors comparing *Gaia* DR2 kinematic information in the solar neighbourhood with simulations including different kinds of spiral arms, representing an agreement of the results using these two different (complementary) datasets.

Given the transient nature of the spiral arms proposed here, where the stellar objects co-rotate with the arm at any radius, we can increase the number of tracers of these spiral arms by adding the youngest OCs (≤30 Myr) to the HMSFRs used to define the present-day arms. As a result, we increase the number of tracers by 314% (adding 264 OCs to the 84 HMSFRs used in Reid et al. 2014), and we report updated parameters for the Perseus, Local, Sagittarius, and Scutum spiral Arms, spanning a wider range in the Galactic azimuth (Table 1).

Acknowledgements. The authors thank the referee for his/her constructive comments that helped improve the paper. ACG thanks Dr. Lennart Lindegren, Dr. Teresa Antoja, Dr. Francesca Figueras, Dr. Maria Monguió and Dr. Pau Ramos for their useful suggestions and comments. ACG also thanks Dr. Louise Howes for her comments on the writing. This work has made use of results from the European Space Agency (ESA) space mission *Gaia*, the data from which were processed by the *Gaia* Data Processing and Analysis Consortium (DPAC). Funding for the DPAC has been provided by national institutions, in particular the institutions participating in the *Gaia* Multilateral Agreement. The *Gaia* mission website is `http://www.cosmos.esa.int/gaia`. The authors are current or past members of the ESA *Gaia* mission team and of the *Gaia* DPAC. This work was (partially) supported by the Spanish Ministry of Science, Innovation and University (MICIU/FEDER, UE) through grants RTI2018-095076-B-C21, ESP2016-80079-C2-1-R, and the Institute of Cosmos Sciences University of Barcelona (ICCUB, Unidad de Excelencia 'María de Maeztu') through grants MDM-2014-0369 and CEX2019-000918-M. ACG acknowledges Spanish Ministry FPI fellowship n. BES-2016-078499. PM gratefully acknowledges support from a research project grant from the Swedish Research Council (Vetenskaprådet). FA is grateful for funding from the European Union's Horizon 2020 research and innovation programme under the Marie Skłodowska-Curie grant agreement No. 800502 H2020-MSCA-IF-EF-2017. This work has received funding from the European Union's Horizon 2020 research and innovation programme under the Marie Skłodowska-Curie grant agreement H2020-MSCA-COFUND-2016-754433. This work has been supported by the Spanish Government (SEV2015-0493), by the Spanish Ministry of Science and Innovation (contract TIN2015-65316-P), by Generalitat de Catalunya (contract 2014-SGR-1051). This research has made use of the VizieR catalogue access tool, CDS, Strasbourg, France. The original description of the VizieR service was published in Ochsenbein et al. (2020).

References

Ahumada, R., Allende Prieto, C., Almeida, A., et al. 2020, ApJS, 249, 3
Anders, F., Chiappini, C., Santiago, B. X., et al. 2014, A&A, 564, A115
Anders, F., Cantat-Gaudin, T., Quadrino-Lodoso, I., et al. 2021, A&A, 645, L2
Antoja, T., Helmi, A., Romero-Gómez, M., et al. 2018, Nature, 561, 360
Bennett, M., & Bovy, J. 2019, MNRAS, 482, 1417
Bovy, J. 2015, ApJS, 216, 29
Buder, S., Asplund, M., Duong, L., et al. 2018, MNRAS, 478, 4513
Cantat-Gaudin, T., Jordi, C., Vallenari, A., et al. 2018, A&A, 618, A93
Cantat-Gaudin, T., Anders, F., Castro-Ginard, A., et al. 2020, A&A, 640, A1
Casamiquela, L., Carrera, R., Jordi, C., et al. 2016, MNRAS, 458, 3150
Castro-Ginard, A., Jordi, C., Luri, X., et al. 2018, A&A, 618, A59
Castro-Ginard, A., Jordi, C., Luri, X., Cantat-Gaudin, T., & Balaguer-Núñez, L. 2019, A&A, 627, A35
Castro-Ginard, A., Jordi, C., Luri, X., et al. 2020, A&A, 635, A45

Dias, W. S., & Lépine, J. R. D. 2005, ApJ, 629, 825
Dias, W. S., Monteiro, H., Lépine, J. R. D., & Barros, D. A. 2019, MNRAS, 486, 5726
Dobbs, C., & Baba, J. 2014, PASA, 31, e035
Dobbs, C. L., & Pringle, J. E. 2010, MNRAS, 409, 396
Drimmel, R., & Spergel, D. N. 2001, ApJ, 556, 181
Eilers, A.-C., Hogg, D. W., Rix, H.-W., et al. 2020, ApJ, 900, 186
Gaia Collaboration (Brown, A. G. A., et al.) 2018a, A&A, 616, A1
Gaia Collaboration (Katz, D., et al.) 2018b, A&A, 616, A11
Gaia Collaboration (Brown, A. G. A., et al.) 2021, A&A, 649, A1
Gerhard, O. 2011, Mem. Soc. Astron. It. Suppl., 18, 185
Grand, R. J. J., Kawata, D., & Cropper, M. 2012, MNRAS, 421, 1529
Gravity Collaboration (Abuter, R., et al.) 2019, A&A, 625, L10
Honig, Z. N., & Reid, M. J. 2015, ApJ, 800, 53
Hunt, J. A. S., Hong, J., Bovy, J., Kawata, D., & Grand, R. J. J. 2018, MNRAS, 481, 3794
Hunt, J. A. S., Johnston, K. V., Pettitt, A. R., et al. 2020, MNRAS, 497, 818
Junqueira, T. C., Chiappini, C., Lépine, J. R. D., Minchev, I., & Santiago, B. X. 2015, MNRAS, 449, 2336
Kamdar, H., Conroy, C., Ting, Y. S., & El-Badry, K. 2020, ApJ, submitted [arXiv:2007.10990]
Katz, D., Sartoretti, P., Cropper, M., et al. 2019, A&A, 622, A205
Kawata, D., Hunt, J. A. S., Grand, R. J. J., Pasetto, S., & Cropper, M. 2014, MNRAS, 443, 2757
Kounkel, M., Covey, K., & Stassun, K. G. 2020, AJ, 160, 279
Lada, C. J., & Lada, E. A. 2003, ARA&A, 41, 57
Lin, C. C., & Shu, F. H. 1964, ApJ, 140, 646
Liu, L., & Pang, X. 2019, ApJS, 245, 32
Liu, C., Wang, Y.-G., Shen, J., et al. 2017, ApJ, 835, L18
Meidt, S. E., Rand, R. J., Merrifield, M. R., Shetty, R., & Vogel, S. N. 2008, ApJ, 688, 224
Mermilliod, J. C., Mayor, M., & Udry, S. 2008, A&A, 485, 303
Mermilliod, J.-C., Mayor, M., & Udry, S. 2009, A&A, 498, 949
Michtchenko, T. A., Lépine, J. R. D., Pérez-Villegas, A., Vieira, R. S. S., & Barros, D. A. 2018, ApJ, 863, L37
Monguió, M., Grosbøl, P., & Figueras, F. 2015, A&A, 577, A142
Monguió, M., Negueruela, I., Marco, A., et al. 2017, MNRAS, 466, 3636
Naoz, S., & Shaviv, N. J. 2007, New Astron., 12, 410
Nordström, B., Mayor, M., Andersen, J., et al. 2004, A&A, 418, 989
Ochsenbein, F., Bauer, P., & Marcout, J. 2000, A&AS, 143, 23
Pringle, J. E., & Dobbs, C. L. 2019, MNRAS, 490, 1470
Quillen, A. C. 2002, AJ, 124, 924
Quillen, A. C., Dougherty, J., Bagley, M. B., Minchev, I., & Comparetta, J. 2011, MNRAS, 417, 762
Quillen, A. C., Carrillo, I., Anders, F., et al. 2018, MNRAS, 480, 3132
Quillen, A. C., Pettitt, A. R., Chakrabarti, S., et al. 2020, MNRAS, 499, 5623
Ramos, P., Antoja, T., & Figueras, F. 2018, A&A, 619, A72
Randich, S., Gilmore, G., & Gaia-ESO Consortium. 2013, The Messenger, 154, 47
Reid, M. J., & Brunthaler, A. 2020, ApJ, 892, 39
Reid, M. J., Menten, K. M., Brunthaler, A., et al. 2014, ApJ, 783, 130
Reid, M. J., Menten, K. M., Brunthaler, A., et al. 2019, ApJ, 885, 131
Roberts, W. W. 1969, ApJ, 158, 123
Roca-Fàbrega, S., Valenzuela, O., Figueras, F., et al. 2013, MNRAS, 432, 2878
Schönrich, R., Binney, J., & Dehnen, W. 2010, MNRAS, 403, 1829
Sellwood, J. A., & Carlberg, R. G. 2014, ApJ, 785, 137
Sellwood, J. A., Trick, W. H., Carlberg, R. G., Coronado, J., & Rix, H.-W. 2019, MNRAS, 484, 3154
Shabani, F., Grebel, E. K., Pasquali, A., et al. 2018, MNRAS, 478, 3590
Shu, F. H. 2016, ARA&A, 54, 667
Sim, G., Lee, S. H., Ann, H. B., & Kim, S. 2019, J. Korean Astron. Soc., 52, 145
Soubiran, C., Jasniewicz, G., Chemin, L., et al. 2018, A&A, 616, A7
Speights, J. C., & Westpfahl, D. J. 2012, ApJ, 752, 52
Steinmetz, M., Matijevič, G., Enke, H., et al. 2020, AJ, 160, 82
Tarricq, Y., Soubiran, C., Casamiquela, L., et al. 2021, A&A, 647, A19
Toomre, A. 1964, ApJ, 139, 1217
Wada, K., Baba, J., & Saitoh, T. R. 2011, ApJ, 735, 1
Worley, C. C., de Laverny, P., Recio-Blanco, A., et al. 2012, A&A, 542, A48
Xu, Y., Reid, M., Dame, T., et al. 2016, Sci. Adv., 2, e1600878
Zwitter, T., Kos, J., Chiavassa, A., et al. 2018, MNRAS, 481, 645